LES modeling for lifted turbulent jet flames

By Luc Vervisch[1] AND Arnaud Trouvé[2]

The LES method is an attractive approach for the simulation of turbulent jet flames. In this method, the effects of large scale structures controlling the mixing process are resolved while small-scale effects such as the leading-edge flames involved in the flame base dynamics are accounted for by the subgrid-scale models. The LES approach is examined in this study with a particular emphasis on a simple formulation for combustion based on the assumption of infinitely fast chemistry. When applied to the problem of turbulent jet flames, this formulation is limited to the description of a regime where the flame remains attached to the fuel injector. Using DNS and LES databases, a modification of the infinitely fast chemistry formulation is proposed in the present study with the objective of numerically capturing transitions to the lifted flame regime and the flame blowout regime. The DNS database corresponds to leading-edge flames evolving in isotropic turbulent flow and is used to describe the structure of the flame base. The LES database corresponds to the near-field region of plane turbulent jets and is used to describe the turbulent mixing process. Preliminary results from *a priori* tests of the new subgrid-scale combustion model are found to be encouraging.

1. Introduction

The model problem of a gaseous fuel jet flowing into a reservoir of air is a generic configuration in combustion theory that has many of the ingredients found in practical non-premixed combustion systems. The numerical simulation of this configuration remains a difficult task, however, for standard Reynolds-Averaged Navier-Stokes (RANS) methods. Indeed, RANS models have difficulties in describing the complex coupling between mixing and chemical reaction that occurs in turbulent jet flames. This coupling leads to 3 possible regimes for flame stabilization: (1) the attached flame regime where the flame is anchored to the fuel injector; (2) the lifted flame regime where the flame is stabilized further downstream at a finite distance from the fuel injector; and (3) the flame blowout regime where the flame cannot be stabilized. Liftoff heights and blowout velocities are quantities of practical engineering interest, and their prediction remains a great challenge for current CFD tools.

The difficulties of RANS models in describing the stabilization region of turbulent jet flames is in part due to the conflicting underlying theories for this problem. The theories differ in the following important aspects (Pitts 1988): (1) the

1 INSA and UMR-CNRS-6614-CORIA, Rouen, France, vervisch@coria.fr
2 Institut Francais du Pétrole, Rueil-Malmaison, France, arnaud.trouve@ifp.fr

degree of premixing upstream of the flame base (for instance Vanquickenborne & van Tiggelen (1966) assume full premixing between fuel and air, whereas Peters & Williams (1983) consider that fuel/air premixing remains negligible); (2) the controlling mechanism for flame stabilization (turbulent premixed flame propagation according to Vanquickenborne & van Tiggelen (1966); laminar diffusion flamelet quenching according to Peters & Williams (1983); large scale turbulent mixing of cold reactants with hot burnt products according to Broadwell *et al.* (1984); turbulent propagation of triple flamelets in partially premixed reactants according to Müller *et al.* (1994)).

Consistent with some aspects of current theories, experimental evidence emphasizes the role of large-scale vortex structures that control the mixing process in the turbulent jet. They also emphasize the role of small-scale, laminar-like, leading-edge (triple) flames that control the flame base motion process (Muñiz & Mungal 1997). Both RANS and large-eddy simulation (LES) approaches have difficulty in capturing leading edge phenomena. In RANS formulations, however, these large- and small-scale effects are not decoupled and remain in the models. It can be argued that this coupling accounts in part for the deficiencies of RANS models. In contrast, the LES approach resolves the large scale structures and only small-scale effects need to be modeled.

Therefore, the ability of LES methods to numerically capture the properties of the unsteady large scales is an attractive feature that allows a new look on the problem of simulating turbulent jet flames (Cook & Riley 1994, Réveillon & Vervisch 1996, Pierce & Moin 1998, Réveillon & Vervisch 1998, Jaberi & James 1998). As far as subgrid-scale modeling is concerned, the standard first step is to assume that the chemical processes are infinitely fast. In this situation, the knowledge of the extent of mixing between fuel and oxidizer is sufficient to fully describe the diffusion flame (Burke & Schumann 1928). The mixing field is characterized using the classical concept of a mixture fraction Z ($Z = 1$ in the fuel feeding stream, $Z = 0$ in the oxidizer reservoir). The temperature and species mass fractions are known functions of Z, and the Z-field is simply obtained in the LES computations from a presumed statistical distribution (via for instance a beta-function probability density function (pdf) $\widetilde{P}(Z)$, where $\widetilde{P}(Z)$ is parametrized in terms of the first and second moments of the Z-distribution, see Libby and Williams 1994).

While the assumption of infinitely fast chemistry remains a valuable first step in applying the LES approach to non-premixed flames, it has also some well-known deficiencies. For instance, Fig. 1 shows that this assumption leads to a flame that is always attached to the fuel injector. For problems where it is important to account for phenomena such as ignition or flame stabilization, the infinitely fast chemistry assumption cannot be invoked, and some alternative description of the turbulent flame must be used.

In the following, we use DNS of leading-edge flames evolving in isotropic turbulent flow and LES of the near-field region of plane turbulent jets. The DNS data are used to describe the structure of the flame base (§2) and to propose a new subgrid-scale combustion model for flame stabilization (§3). The LES data are used to describe

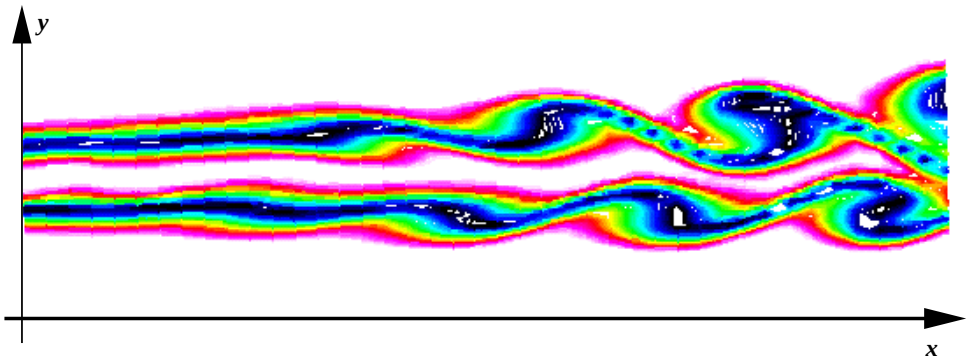

FIGURE 1. LES results of the near-field region of a plane turbulent jet flame. Instantaneous snapshot showing isocontours of the LES-filtered temperature in a constant z-plane. The LES formulation uses the assumption of infinitely fast chemistry, and the simulations are, therefore, limited to a description of the attached flame regime. This simulation was performed using the LES code presented in §4.

the turbulent mixing process and to examine the behavior of the turbulent mixing time scale that is used by the combustion sub-model (§4).

2. DNS of a turbulent edge-flame

2.1 Introduction

Focusing on the stabilization region of turbulent flames implies studying the point where the transition from non-burning to burning occurs (Muñiz & Mungal 1997). In a non-premixed situation, this transition is related to the appearance of edge-flames (Vervisch & Poinsot 1998). Experimental studies of the structure of the edge of diffusion flames have suggested that partially premixed combustion controls the properties of those edges (Phillips 1965, Kioni *et al.* 1993, Plessing *et al.* 1998). A possible model problem for partially premixed combustion is the triple flame configuration composed of a curved partially premixed flame front followed by a trailing diffusion flame. The triple flame analogy has been an effective tool to gain some understanding on the properties of propagation of diffusion flames (Hartley & Dold 1991, Veynante *et al.* 1994, Ruetsch *et al.* 1995, Ghosal & Vervisch 1998), the role of partially premixed combustion in auto-ignition problems (Domingo & Vervisch 1996), the chemical structure of the edge of diffusion flames (Echekki & Chen 1998), and diffusion flame holding (Buckmaster & R. Weber 1996) together with the effects of edge flames in liftoff situations (Favier & Vervisch 1998).

To increase our basic understanding and help the modeling of liftoff in non-premixed jet flames, we use direct numerical simulations of the edge of a diffusion flame interacting with freely decaying turbulence. The calculation starts with the establishment of a fully compressible laminar triple flame, using one-step chemistry and following the procedure proposed by Ruetsch *et al.* (1995) for unity Lewis

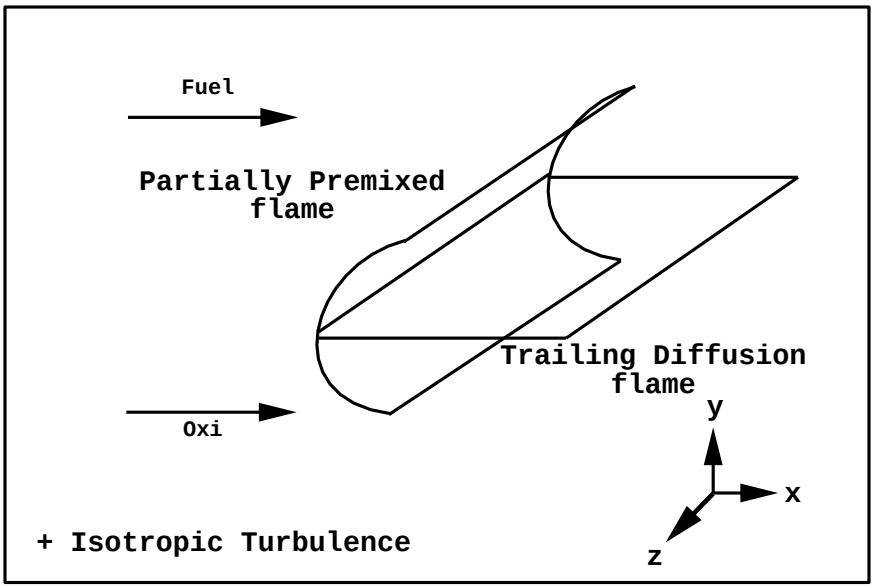

FIGURE 2. Sketch of the DNS configuration corresponding to the edge of a diffusion flame interacting with isotropic turbulence.

number. A three-dimensional initial condition for the mixture and the velocity field is obtained by repeating the two-dimensional triple flame in the spanwise direction z (Fig. 2). The flame is then allowed to interact with the turbulence. The DNS solver follows the methodology of Poinsot *et al.* (1996). We refer the reader to Domingo & Vervisch (1996) for more details on the solver. The DNS database include two synthetic problems corresponding to different characteristic length and time scales of the flame-flow interaction (see Table 1). Case I corresponds to the edge of a diffusion flame interacting with vortices that are large compared to the characteristic length of the flame, while case II is representative of an interaction with a more energetic turbulence, in which more scales are present.

Case	δ_m/l_t	δ_R/l_t	$u^{'}/S_l^o$	$u^{'}/S_{TF}^o$	Re_{lt}
I	0.10	0.25	5.64	3.64	157
II	0.20	0.40	11.3	7.30	125

Table 1. Parameters of the simulations ($129 \times 129 \times 65$). The initial laminar triple flame propagates with a velocity S_{TF}^o in a mixing zone of thickness δ_m, while the thickness of the reaction zone in the trailing diffusion flame is δ_R. The propagation speed of the stoichiometric mixture is S_l^o. The temperature ratio between fully burnt stoichiometric mixture and fresh gases is set to 4, and the stoichiometric composition corresponds to $Z_{st} = 0.5$. The turbulence is characterized by its integral length scale l_t, the amplitude $u^{'}$ of the velocity fluctuation, and the turbulent Reynolds number $Re_{l_t} = (u^{'} l_t/\nu)$.

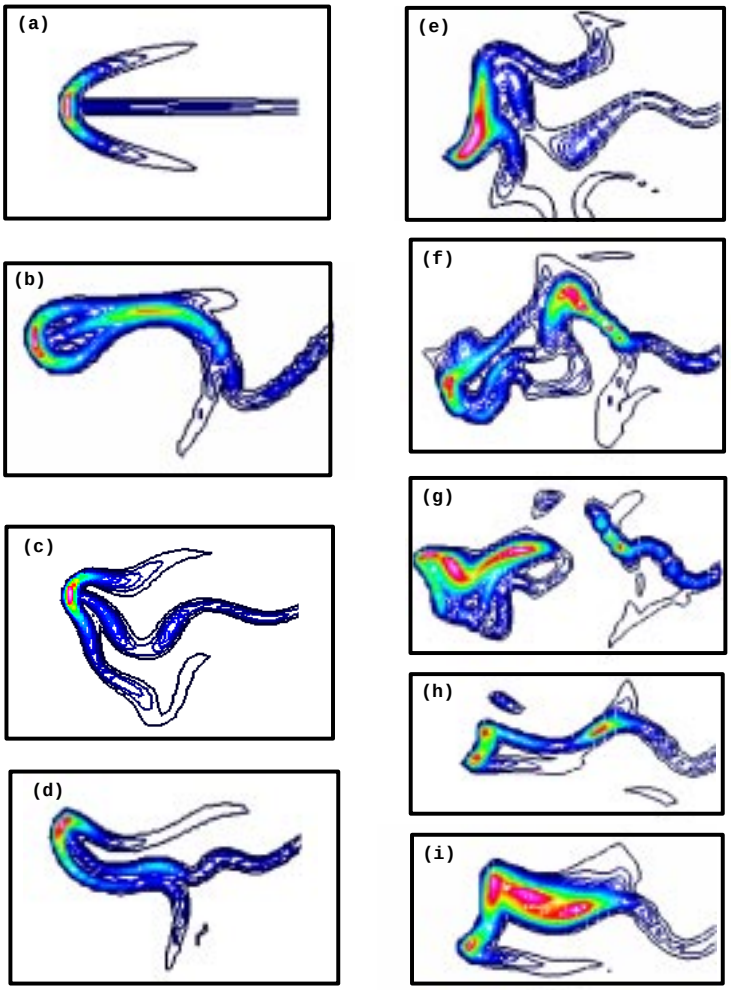

FIGURE 3. Instantaneous snapshots showing isocontours of the reaction rate in different constant z-planes. Initial laminar triple flame: (a); Case I: (b) - (c) - (d); Case II: (e) - (f) - (g) - (h) - (i).

2.2 Topology of the turbulent edge flame

After two eddy turn-over times, the turbulent mixing of the reactants is fully developed, and the initially laminar triple flame has evolved into the edge of a non-premixed turbulent flame. Instantaneous snapshots of the reaction zone reveal a complex structure (Fig. 3), showing that the partially premixed front and the trailing diffusion flame have been strongly modified by the turbulence. This is particularly true in case II (Figs. 3e-i) where the flame is exposed to intense turbulence.

One basic effect of the turbulent flow is to produce a number of zones with high values of the reaction rate at the extremity of the main body of the diffusion flame. The multiplication of these chemically super-active regions appears as the result of two mechanisms: (1) the development of a turbulent partially premixed front with a flame surface that is wrinkled by the vorticity field; (2) the stretching of the diffusion

flame due to local high levels of the scalar dissipation rate. Diffusion flame stretching tends to locally increase the burning rate. It may also lead to local quenching of the diffusion flame, generating new edges that are in turn associated with high burning rates. The first mechanism above is illustrated in Fig. 3f, displaying a plane where the edge of the reaction zone is composed of two stoichiometric points, each being supported by a turbulent partially premixed front and followed by a trailing diffusion flame. The possible increase of the burning rate in the trailing diffusion flame (the second mechanism above) is visible in Fig. 3b where the diffusion flame is pinched by a pair of vortices, also pushing the wings of the partially premixed front towards the diffusion flame. The second mechanism with local quenching of the diffusion flame may be observed in Fig. 3g, where the quenching is responsible for the development of a partially premixed kernel isolated from the downstream diffusion flame.

Despite the complexity of the fine scale structure of these flames, it is important to note that the turbulent edge of the reaction zone is always composed, in the mean, of a turbulent partially premixed front followed by a turbulent trailing diffusion flame. This fact becomes obvious when studying the flame structure in mixture fraction space.

2.3 The structure of laminar and turbulent edge flames in mixture fraction space

We now analyze the flame structure at a given time by averaging all quantities in the homogeneous spanwise direction z and considering that these averaged quantities are functions of the streamwise and cross-stream coordinates x and y. Profiles of fuel mass fraction $Y_F(x, y)$, temperature $T(x, y)$, and reaction rate $\dot{\omega}(x, y)$ are plotted versus the mixture fraction $Z(x, y)$ in Figs. 4 and 5, for various streamwise locations. Figure 4 corresponds to the analysis of the initial laminar triple flame; Fig. 5 to the analysis of the turbulent flame.

In mixture fraction space, the fuel mass fraction profile $Y_F(Z)$ lies between the limit of mixing without reaction, corresponding to $Y_F = Z$, and the infinitely fast chemistry limit, corresponding to $Y_F = 0$ for $Z \leq Z_{st}$ and $Y_F = (Z - Z_{st})/(1 - Z_{st})$ for $Z > Z_{st}$. Note that the reference problem for non-premixed combustion is the strained counter-flowing fuel/oxidizer diffusion flame (Peters 1986). In this model problem, the mixing of the reactants occurs together with their consumption, and the pure mixing line $Y_F = Z$ cannot be observed (except under quenching conditions). This is not the case when the edge of the diffusion flame is composed of a partially premixed front where some cold premixing of the reactants must take place prior to combustion. As a consequence, the structure in mixture fraction space of the edge flame is expected to be different from that observed in a counter-flowing fuel/oxidizer diffusion flame.

This is confirmed by the present DNS in both the laminar and the turbulent flame configurations. First, we observe a preheating region (curves marked by circles in Figs. 4 and 5) developing in the vicinity of the stoichiometric triple point. Then, as we move downstream from the partially premixed front into the trailing diffusion flame, we observe that for conditions close to stoichiometry, $Z = Z_{st}$, the fuel mass fraction decays from $Y_F = Z_{st}$ to $Y_F = 0$. In this transition region, the fluid particles coming from the oxidizer stream ($Z = 0$) always undergo some premixing with fuel

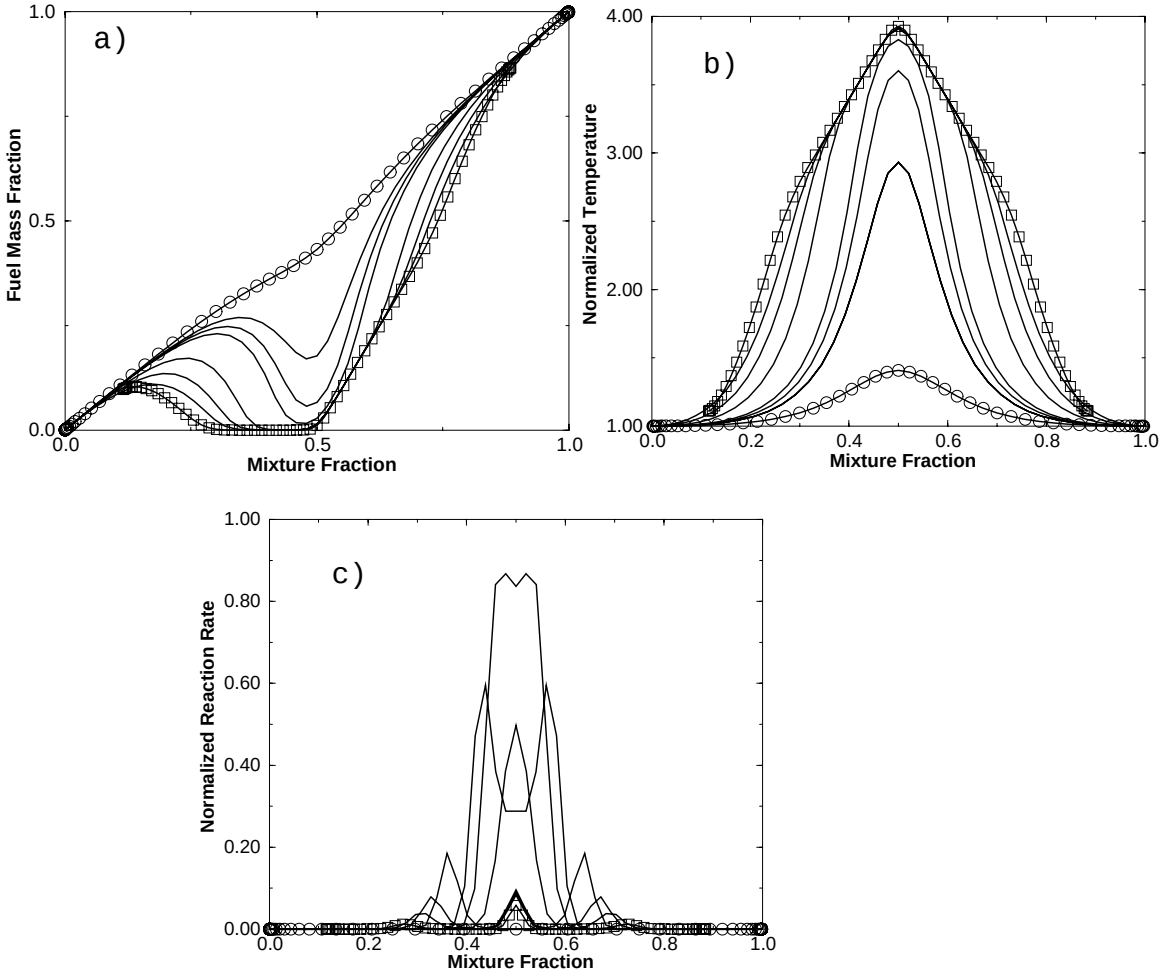

FIGURE 4. Fuel mass fraction (a), temperature (b), and reaction rate (c) plotted versus mixture fraction at various streamwise positions x of a laminar edge-flame configuration (Fig. 3a). $\circ$: x is slightly upstream of the flame and serves to describe the preheat zone; $\square$: x is downstream of the triple point and serves to describe the trailing diffusion flame. Temperature and reaction rate are respectively normalized with the temperature of the fresh gases and with the maximum reaction rate in a stoichiometric plane laminar flame.

before reaching the diffusion flame at $Z = Z_{st}$. Similarly, the fluid particles coming from the fuel stream ($Z = 1$) always undergo some premixing with oxidizer before reaching the diffusion flame at $Z = Z_{st}$.

When the triple flame interacts with the turbulent flow, large differences are observed between the laminar and turbulent cases for the profiles of reaction rate (compare Fig. 4 right with Fig. 5 bottom right). In contrast, the results show that the profiles of fuel mass fraction are similar in the laminar and turbulent cases if considered in $Z-$space. These profiles can be considered as more generic, and we now use this result to propose a skeletal description of the turbulent edge-flame in mixture fraction space.

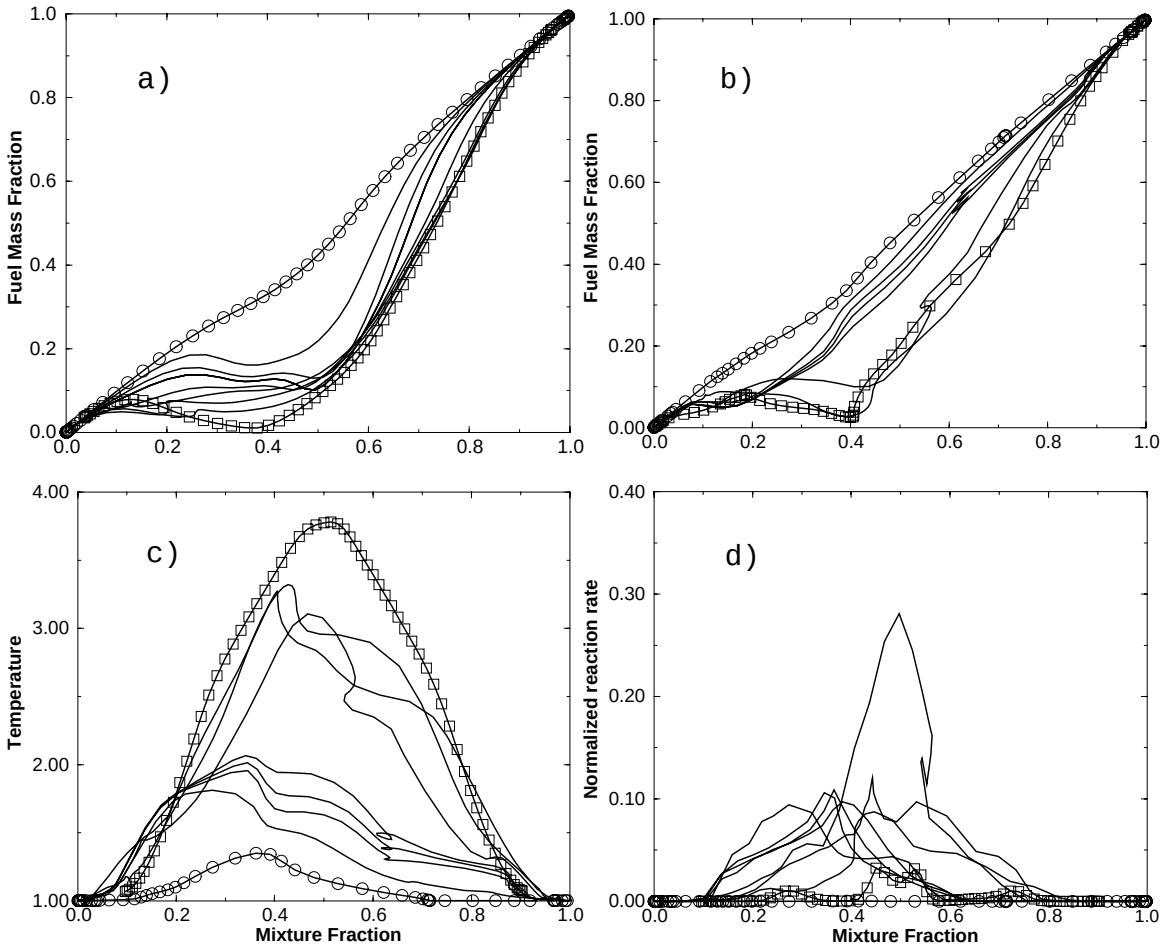

FIGURE 5. Fuel mass fraction in case I (a) and case II (b), temperature (c) and reaction rate (d) plotted versus mixture fraction at various streamwise positions x of a turbulent edge-flame configuration (Fig. 3). $\circ$: x is slightly upstream of the flame and serves to describe the preheat zone; $\square$: x is downstream of the triple point and serves to describe the trailing diffusion flame. Temperature and reaction rate are respectively normalized with the temperature of the fresh gases and with the maximum reaction rate in a stoichiometric plane laminar flame.

3. Simple EDge Flame Model (SEDFM)

3.1 Introduction

Flame stabilization results from complex interactions between the edge flames previously discussed and the large scale coherent structures present in the turbulent flow. The state of the art in LES of combustion chambers is based on the use of the Infinitely Fast Chemistry Model (IFCM) (Pierce & Moin 1998). With infinitely fast chemistry, the fuel mass fraction is calculated by presuming the probability density function of the mixture fraction $\widetilde{P}(Z;\underline{x},t)$ from its first and second moments, $\widetilde{Z}$ and $\widetilde{Z''^2}$, as obtained from the resolution of the large eddy field. The LES-resolved fuel mass fraction is then computed as $\widetilde{Y}_F(\underline{x},t) = \int_0^1 Y_F^{IFCM}(Z)\widetilde{P}(Z;\underline{x},t)dZ$, where

$Y_F^{IFCM}(Z)$ is the equilibrium structure of the flame in mixture fraction space (Fig. 6 top). To include finite rate chemistry effects in LES, we propose to conserve this simple and attractive formalism by simply replacing $Y_F^{IFCM}(Z)$ by a modified function accounting for the presence of edge flames. This new flame structure in mixture fraction space is parametrized using a partially stirred reactor subgrid model.

3.2 Skeletal description of turbulent edge flames

The infinitely fast chemistry assumption makes Y_F a piecewise linear function of Z. In Fig. 6 (top figure), this function is constructed from three points A, C, and E, defined by their (Z, Y_F) coordinates: $A(0,0)$; $C(Z_{st},0)$; $E(1,Y_{F,o})$ (the subscript o denotes a concentration taken in the feeding stream of fuel or oxidizer).

We propose to improve this skeletal description of the flame by introducing two additional points B and D located on the pure mixing line $Y_F = Z$. We thereby allow for variable, non-zero concentration of fuel at point C corresponding to stoichiometric conditions (Fig. 6 bottom). In this new skeletal structure, the limit of pure mixing is obtained when B, C, and D are such that $Y_{F_B} = Y_{F_C} = Y_{F_D} = Z_{st}$ (Fig. 6 bottom left); the limit of equilibrium chemistry is obtained when $B = A$, $D = E$, and C is such that $Y_{F_C} = 0$. Finite rate chemistry effects with edge flames are mimicked by letting the skeletal structure evolve from the pure mixing case to the equilibrium chemistry case. In the SEDFM model, we choose to meet this requirement by using the relations presented in Table 2. These relations give the flame structure in mixture fraction space as a function of a single parameter Y_{F_C}.

$\mathbf{Z}$	$\mathbf{Y_F^{SEDFM}(Z)} =$
$Z \leq Y_{F_B}$	Z
$Y_{F_B} < Z \leq Z_{st}$	$(Z - Y_{F_B})(Y_{F_C} - Y_{F_B})/(Z_{st} - Y_{F_B}) + Y_{F_B}$
$Z_{st} < Z \leq Y_{F_D}$	$(Z - Z_{st})(Y_{F_D} - Y_{F_C})/(Y_{F_D} - Z_{st}) + Y_{F_C}$
$Y_{F_D} < Z$	Z
$Y_{F_B} = (Z_{st}^2 - (Y_{F_C} - Z_{st})^2)^{1/2}$ and $Y_{F_D} = (1 - Z_{st})(Z_{st} - Y_{F_B})/Z_{st} + Z_{st}$	

Table 2: Flame structure in mixture fraction space in the SEDFM model.

The fuel concentration at point C may be viewed as a measure of the conditional mean value of fuel mass fraction at $Z = Z_{st}$, $Y_{F_C} = \left(\overline{Y_F \mid Z = Z_{st}}\right)$ (Smith 1996). Figure 7 shows a test of the model where Y_{F_C} has been extracted from the DNS. The results indicate that this skeletal description is an acceptable compromise to describe the flame in mixture fraction space including finite rate chemistry effects. We now turn to the yet unspecified parameter of the model: the conditional fuel mass fraction Y_{F_C}.

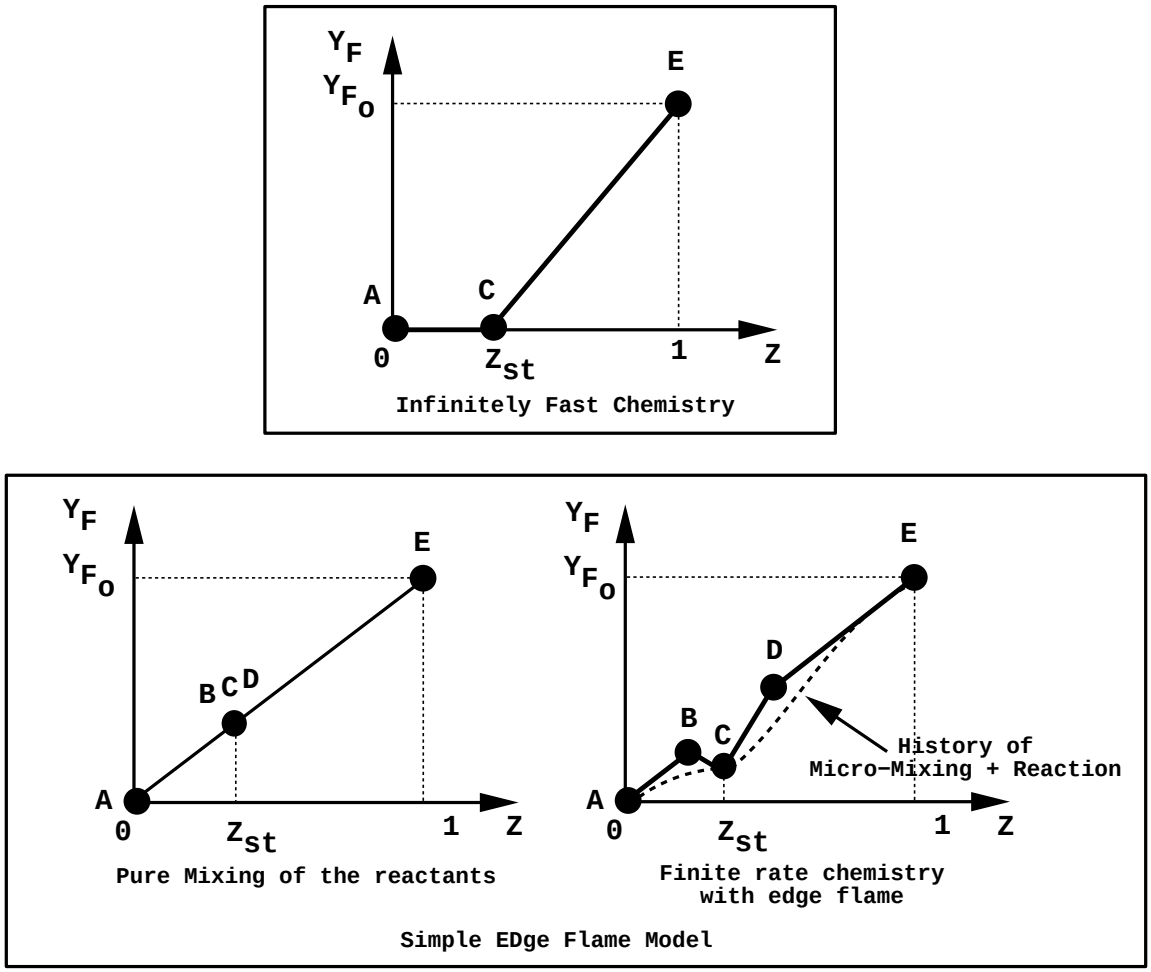

FIGURE 6. Skeletal description of the turbulent edge-flame in the SEDFM model.

3.3 Subgrid-scale reactor modeling to determine Y_{F_C}

Broadwell & Lutz (1998) have recently proposed a model for the production of NO_x in turbulent jet flames based on a description of chemical reaction at every axial location by a partially stirred reactor. Along the same lines, Borghi (1988) has proposed various turbulent combustion models using trajectories in composition space, and Ravet & Vervisch (1998) have developed a multi-level pdf-generator for RANS simulations of aeronautical engines. We follow the same approach for determining Y_{F_C}, the key parameter of SEDFM.

At each LES mesh point and at every time step t, the conservation equation of fuel mass evolving in a partially stirred reactor (PaSR) may be cast in the form:

$$\frac{dY_F}{dZ} = \frac{(\widetilde{Y}_F^t - Y_F) + \widetilde{\tau}^t \dot{\omega}(Y_F, Z)}{(\widetilde{Z}^t - Z)} \quad , \tag{1}$$

where $\widetilde{Y}_F^t$ and $\widetilde{Z}^t$ are respectively the known LES-filtered fuel mass fraction and mixture fraction. The subgrid mixing time $\widetilde{\tau}^t$ is estimated from the resolved flow

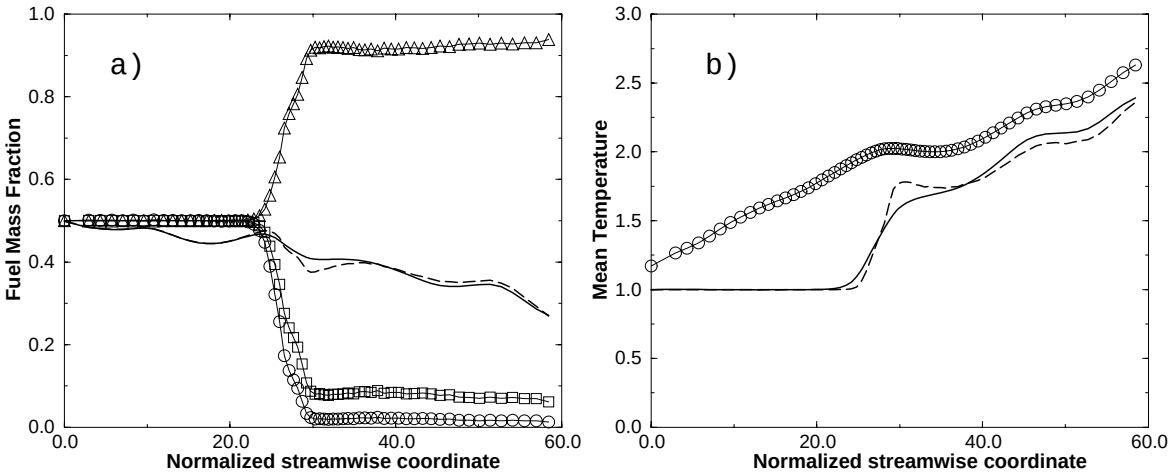

FIGURE 7. *A priori* test of the SEDFM model. a): streamwise variations of the fuel mass fraction at points B, C and D in the SEDFM model. Comparison between the SEDFM model and the DNS data for the mean (spanwise and cross-stream averaged) fuel mass fraction. $\circ$: Y_{F_C}; $\square$: Y_{F_B}; $\triangle$: Y_{F_D}; - - - - : SEDFM; ——— : DNS. b): Comparison between the SEDFM model, the IFCM model, and the DNS data for the mean (spanwise and cross-stream averaged) temperature. The x-coordinate is normalized with the thickness of the premixed stoichiometric plane laminar flame. ——— : DNS; $\circ$: IFCM; - - - - : SEDFM.

field (see §4), and finite rate chemistry effects enter the model via $\dot{\omega}(Y_F, Z)$ given for instance by a one-step finite rate chemical scheme.

The solution of the PaSR equation (1) gives $Y_F^{PaSR}(Z)$, a fuel trajectory in Z-space accounting for the interaction between subgrid-scale micro-mixing and chemical reaction. Indeed when $(\widetilde{\tau}^t\dot{\omega})/(\widetilde{Y}_F^t - Y_F) \gg 1$, the solution of (1) approaches the infinitely fast chemistry solution $Y_F^{IFCM}(Z)$. In addition, when $\widetilde{\tau}^t \to 0$, the solution of (1) approaches the mixing line solution, $Y_F = Z$. Since our objective is to determine Y_{F_C}, only half of the trajectory needs to be computed: for fuel rich conditions ($\widetilde{Z} > Z_{st}$) the PaSR equation is solved with the initial condition on the fuel lean side ($Z = 0, Y_F = 0$), whereas for fuel lean conditions ($\widetilde{Z} < Z_{st}$) the initial condition is taken on the fuel rich side ($Z = 1, Y_F = Y_{F,o}$). In both cases the point $Y_F^{PaSR}(Z_{st})$ determines Y_{F_C}, and thereby the new fuel concentration $\widetilde{Y}_F^{t+\delta t}$ using the flame structure $Y_F^{SEDFM}(Z)$ discussed above.

Note that Eq. (1) is similar to the equation solved for the trajectory of a Monte-Carlo particle in Z-space as obtained from a pdf method using the LMSE mixing closure (Pope 1985, Dopazo 1994). This equation can also be understood as a local dynamic subgrid flamelet where the contribution of diffusion, $D\nabla^2 Y_F$, is modeled as a linear relaxation term: $(\widetilde{Y}_F - Y_F)/\overline{\tau}$.

4. LES of the near-field region of plane turbulent jets

The LES simulations are performed using a three-dimensional, compressible Navier-Stokes solver. The solver features a high-order finite difference scheme that is sixth-order accurate in space (Lele 1992) and third-order in time. It is similar to the DNS solver used for the direct simulations of turbulent leading-edge flames (§2). Boundary conditions are specified with the NSCBC method proposed by Poinsot & Lele (1992). The LES formulation corresponds to the subgrid-scale (SGS) models proposed by Moin *et al.* (1991). The SGS models are variants of the Smagorinsky model based on an eddy-diffusivity assumption for the momentum, heat and mass SGS turbulent fluxes, and a variant of the Yoshizawa model for the SGS turbulent kinetic energy. While the LES solver may be run using the dynamic procedure proposed by Moin *et al.* (1991), the present simulations are performed using constant model coefficients: $C_S = 0.033$; $C_I = 0.1$; $Pr_t = 0.6$; $Sc_t = 0.8$, where C_S is the standard Smagorinsky coefficient, C_I the Yoshizawa coefficient, Pr_t the SGS turbulent Prandtl number, and Sc_t the SGS turbulent Schmidt number.

The computational configuration corresponds to the near-field region of a three-dimensional plane jet, $0 \leq x/H \leq 20$, where H is the initial jet height. The jet Reynolds number $Re_j \equiv (U_j H/\nu)$ is 6000, with U_j the mean jet inlet velocity and ν the fluid kinematic viscosity. The left x-boundary corresponds to inflow conditions with prescribed velocity and scalar values; the right x-boundary corresponds to outflow conditions, the y-boundaries to non-reflecting conditions ($-5 \leq y/H \leq 5$), and the z-boundaries to periodic conditions ($0 \leq z/H \leq 5$). The mean inlet x-velocity and scalar profiles are given by the following expressions:

$$\widetilde{u}(0,y,z) = \frac{U_j + U_{co}}{2} + \frac{U_j - U_{co}}{2}\ tanh(\frac{H/2 - |y|}{2\theta}) \tag{2}$$

$$\widetilde{Z}(0,y,z) = \frac{1}{2} + \frac{1}{2}\ tanh(\frac{H/2 - |y|}{2\theta}) \tag{3}$$

where θ is the LES-filtered initial thickness of the jet shear layers, U_{co} is a co-flow velocity that is added to maintain convective outflow conditions at the right x-boundary, and $\widetilde{Z}$ is the LES-filtered mixture fraction. In the present study, we use $\theta/H = 0.1$ and $U_{co}/U_j = 1/6$. The jet is also weakly forced at the inlet (left) x-boundary using a NSCBC variant of the random fluctuation method of Lee *et al.* (1992). The jet inlet velocity fluctuations are specified using an auxiliary field corresponding to homogeneous isotropic turbulence and a prescribed model energy spectrum (Passot-Pouquet). The perturbations are characterized by moderate levels of the forcing intensity, $u'/U_j \approx 2\%$, and an integral length scale of $l_t/H \approx 0.5$. Note that the particular implementation of the forcing method used in the present study also induces some weak scalar fluctuations at inlet (see Fig. 8 at $x = 0$). Furthermore, in the present study, the grid spacing is uniform and the resolution is $101 \times 200 \times 50$.

The LES simulations describe the mixing dynamics occurring in the near-field region of the turbulent jet. As shown in Fig. 8, the scalar field in the vicinity of the injector features a dramatic transition from an early stage ($0 \leq x/H \leq$

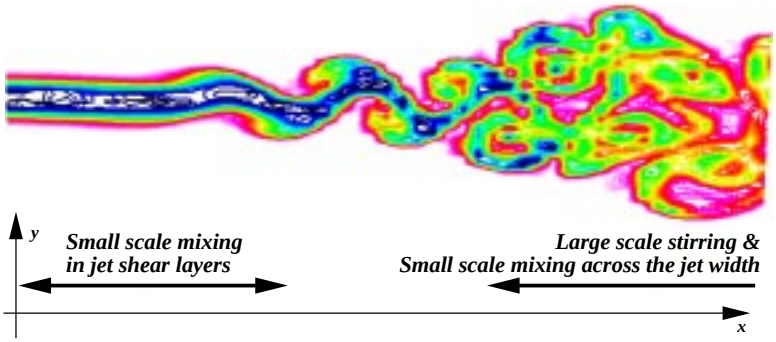

FIGURE 8. Mixing dynamics in the near-field region of a plane turbulent jet. Instantaneous snapshot showing isocontours of the LES-filtered mixture fraction in a constant z-plane.

7), where mixing remains confined within the jet shear layers, to a second stage ($x/H > 7$) characterized by large scale stirring motions. These stirring motions are associated with the jet coherent structures, resulting in faster spreading rates and more distributed small scale mixing across the jet width.

This transition is also observed in Fig. 9 where the mean total and SGS scalar dissipation rates, $< \widetilde{\chi} >$ and $< \widetilde{\chi}_{SGS} >$, are plotted as a function of streamwise location. Following Pierce & Moin (1998), we write:

$$\widetilde{\chi} = \frac{2}{\overline{\rho}} \left(\frac{\overline{\mu}}{Sc} + \frac{\mu_t}{Sc_t}\right) |\nabla \widetilde{Z}|^2 \tag{4}$$

$$\widetilde{\chi}_{SGS} = \frac{2}{\overline{\rho}} \frac{\mu_t}{Sc_t} |\nabla \widetilde{Z}|^2 \tag{5}$$

where $\overline{\rho}$ is the LES-filtered mass density, $\overline{\mu}$ the LES-filtered molecular viscosity, Sc the molecular Schmidt number, and μ_t the Smagorinsky turbulent eddy viscosity. In Fig. 9, these quantities are both spatially averaged in $(y-z)$ planes and time averaged over a period of time: $< \widetilde{\chi} >= (\int \widetilde{\chi}\, dydzdt)/(L_y L_z T)$, where L_y (L_z) is the y-size (z-size) of the computational domain, and T the averaging time period. T corresponds approximately to twice the mean time of flight of a jet fluid particle across the computational domain.

Figure 9 allows some refinement of the two-zone description of mixing presented in Fig. 8. Figure 9 suggests that mixing in the near-field region of the turbulent jet can in fact be described by a sequence of 3 stages: (1) an early stage ($0 \leq x/H \leq 7$) where $< \widetilde{\chi} >$ is approximately constant; (2) an intermediate stage ($7 \leq x/H \leq 15$) where $< \widetilde{\chi} >$ increases; and (3) a fully-developed stage ($x/H > 15$) where $< \widetilde{\chi} >$ decreases. Note that $< \widetilde{\chi} >$ carries information on both the spatial extent of mixing (on the jet thickness) and the local values of the rates of mixing (on the values of $\widetilde{\chi}$). The transition from the first to the second stage is related to the onset of large scale turbulent mixing and a corresponding rapid increase in the turbulent

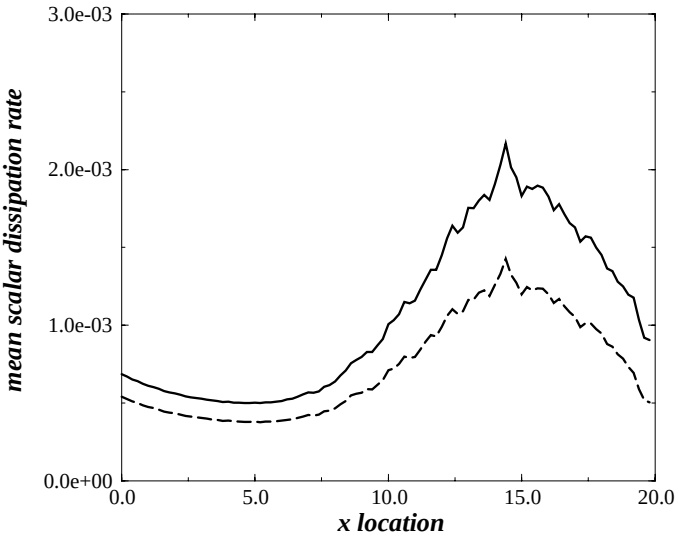

FIGURE 9. Streamwise evolution of the mean total and SGS scalar dissipation rates, $<\widetilde{\chi}>$ (———) and $<\widetilde{\chi}_{SGS}>$ (- - - -) *vs* x. The mean scalar dissipation rates are made non-dimensional with the initial jet time scale, (H/U_j). x is made non-dimensional with the initial jet height H.

jet thickness. The transition from the second to the third fully-developed stage is related to the lower local instantaneous values of the scalar dissipation rate that are found downstream, as the jet fluid is further decelerated and the turbulence levels are progressively reduced.

The downstream evolution from fast to slow SGS mixing rates, as observed in Fig. 9 for $x/H > 15$, is the key mechanism that controls flame stabilization in the LES combustion sub-model proposed in §3. The corresponding key quantity in the SEDFM model is the turbulent mixing time scale $\widetilde{\tau}^t$, and a basic requirement of the model is that $\widetilde{\tau}^t$ increases (at least in a mean sense) with downstream distance. Figure 10 shows that this requirement is correctly met using the local SGS turbulent time scale as an estimate for $\widetilde{\tau}^t$:

$$\widetilde{\tau}^t = \frac{\Delta}{\sqrt{\widetilde{k}_{SGS}}} = \frac{1}{\sqrt{C_I}|\widetilde{S}|} \tag{6}$$

where Δ is the LES filter size, $\Delta \equiv (\Delta_x \Delta_y \Delta_z)^{1/3}$, $\widetilde{k}_{SGS}$ the SGS turbulent kinetic energy, and $|\widetilde{S}| \equiv (2\widetilde{S}_{ij}\widetilde{S}_{ij})^{1/2}$, with $\widetilde{S}_{ij} \equiv (\partial\widetilde{u}_i/\partial x_j + \partial\widetilde{u}_j/\partial x_i)/2$. Note that in Fig. 10, the analysis is conditioned on being in the mixing zone: $\widetilde{\tau}^t$ is conditioned on $|\nabla\widetilde{Z}|$ being larger than a threshold value that corresponds to approximately 20% of the maximum value of the mixture fraction gradient at $x = 0$.

Figure 10 shows a classical evolution from fast to slow time scales for mixing, with $<\widetilde{\tau}^t>$ approximately twice as long at $x/H = 20$ compared to its initial value at $x/H = 0$. This evolution is also observed in Fig. 11 where the pdf of $\widetilde{\tau}^t$ is presented

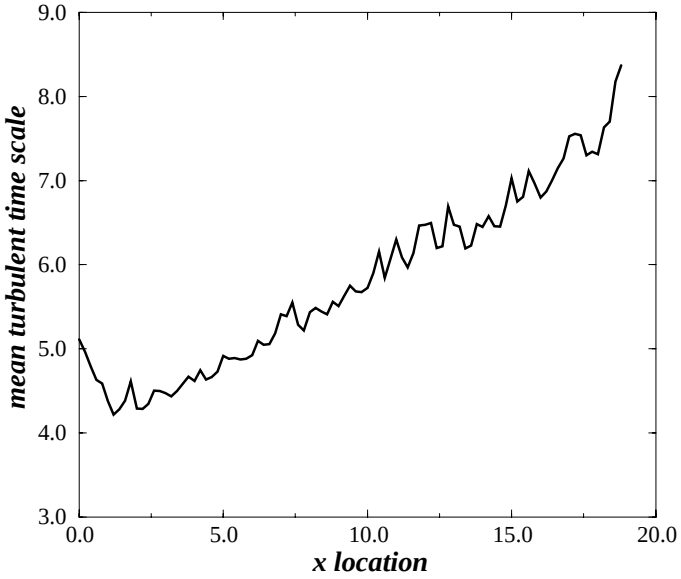

FIGURE 10. Streamwise evolution of the mean SGS turbulence time scale, $< \widetilde{\tau}^t >$ *vs* x. The mean SGS turbulence time scale is made non-dimensional with the initial jet time scale (H/U_j). x is made non-dimensional with the initial jet height H.

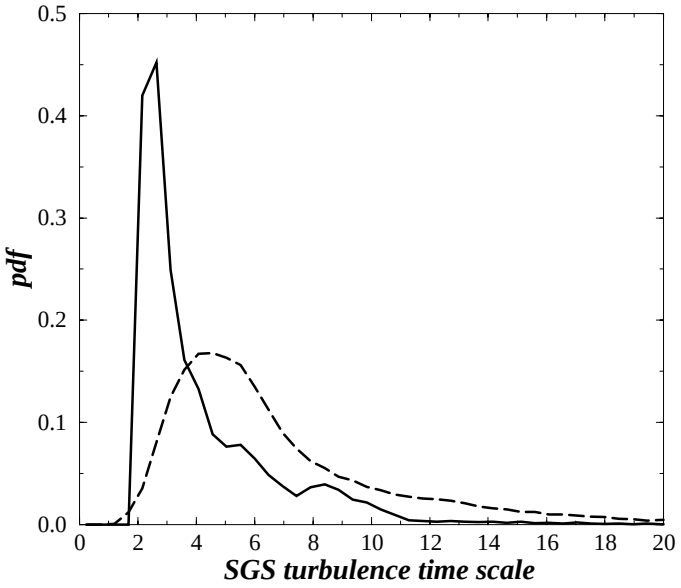

FIGURE 11. Probability distribution of the SGS turbulence time scale, $\widetilde{\tau}^t$, at $x/H = 1.8$ (———) and $x/H = 17.8$ (- - - -). $\widetilde{\tau}^t$ is made non-dimensional with the initial jet time scale, (H/U_j).

at 2 streamwise locations. Figure 11 reveals a weak downstream trend towards wider statistical distributions of mixing time scales. The $\widetilde{\tau}^t$-distribution at $x/H = 17.8$ covers a range of time scales that can vary by an order of magnitude. It is expected that the SEDFM model will be sensitive to the largest values in this distribution

and will allow flame stabilization at grid locations where $\widetilde{\tau}^t$ is sufficiently large.

5. Conclusion

Direct numerical simulations of leading-edge flames evolving in isotropic turbulent flow are used in the present study to propose a new subgrid-scale combustion model (the SEDFM model) for large eddy simulations of the stabilization region of turbulent jet flames. The SEDFM model is based on a skeletal description of the flame structure in mixture fraction space and a transition in that description from the pure mixing line solution to the equilibrium solution. The transition occurs at a rate given by a simple analogy with a partially stirred reactor (PaSR) configuration. The PaSR model measures the relative speeds of subgrid-scale mixing and chemical reaction. The key parameter in the SEDFM model is the turbulent mixing time scale $\widetilde{\tau}^t$.

Large eddy simulations of the near-field region of plane turbulent jets are also used to describe the turbulent mixing process and to propose an estimate of the turbulent mixing time scale $\widetilde{\tau}^t$. It is found that a simple estimate of $\widetilde{\tau}^t$ based on the local subgrid-scale turbulent time scale, $(\Delta/(\widetilde{k}_{SGS})^{1/2})$, is sufficient to describe the downstream evolution from fast to slow mixing rates.

Preliminary results from *a priori* tests of the SEDFM model are found to be encouraging. *A posteriori* tests and a full evaluation of the performance of the model in LES simulations are currently in progress.

Acknowledgment

This work has benefited from many stimulating and exciting discussions with the members of the CTR Summer Program, in particular the authors gratefully acknowledge their CTR hosts Prof. J. Ferziger, Dr. G. Ruetsch, and C. D. Pierce.

REFERENCES

Borghi, R. 1988 Turbulent combustion modeling. *Prog. Energy Combust. Sci.* **14,** 245-292.

Bray, K. N. C. 1996 The Challenge of turbulent combustion. *Twenty-sixth Symp. (Intl.) on Combust.* The Combustion Institute, Pittsburgh**.**

Broadwell, J. E. & Lutz A. 1998 A turbulent jet chemical reaction model: NO_x production in jet flames. *Combust. Flame.* **114,** 319-335.

Broadwell, J. E., Dahm, W. J. A. & Mungal, M. G. 1984 Blowout of turbulent diffusion flames. *Twentieth Symp. (Intl) on Combust.* The Combustion Institute, 303-310.

Buckmaster, J. & Weber, R. 1996 Edge-Flame Holding. *Twenty-sixth Symp. (Intl) on Combust.* The Combustion Institute, Pittsburgh**.**

Burke, S. P. & Schumann, T. E. W. 1928 Diffusion flames. *Industr. Eng. Chem.* **20,** 998-1004.

Cook, A. W. & Riley, J. J. 1994 A subgrid model for equilibrium chemistry in turbulent flows. *Phys. Fluids.* **8**(6)**,** 2868-2870.

Domingo, P. & Vervisch, L. 1996 Triple flames and partially premixed combustion in autoignition of nonpremixed mixtures. *Twenty-sixth Symp. (Intl) on Combust.* The Combustion Institute, Pittsburgh**.**

Dopazo, C. 1994 Recent developments in pdf methods. *In Turbulent Reacting Flows.* (ed. P. A. Libby & F. A. Williams). Academic Press London, 375-474.

Echekki, T. & Chen, J. H. 1998 Structure and propagation of methanol-air triple flames. *Combust. Flame.* **114,** 231-245.

Favier, V. & Vervisch, L. 1998 Investigating the effects of edge-flames in liftoff in non-premixed turbulent combustion. *Twenty-seventh Symp. (Intl) on Combust.* The Combustion Institute, Pittsburgh**.**

Ghosal, S. & Vervisch, L. 1998 Asymptotic theory of triple flame including effects of heat release. Submitted to *J. Fluid Mech.*

Hartley, L. J. & Dold, J. W. 1991 Flame propagation in a nonuniform mixture: analysis of a propagating triple-flame. *Combust. Sci. Tech.* **80,** 23-46.

Jaberi, F. A. & James, S. 1998 A dynamic similarity model for large eddy simulation of turbulent combustion. *Phys. Fluids.* **10**(7)**,** 1775-1777.

Kioni, P. N., Rogg, B., Bray K.N.C. & Liñán, A. 1993 Flame spread in laminar mixing layers: the triple flame. *Combust. Flame.* **95,** 276.

Lee, S., Lele, S. K. & Moin, P. 1992 Simulation of spatially evolving turbulence and the applicability of Taylor's hypothesis in compressible flow. *Phys. Fluids A.* **4,** 1521.

Lele, S. K. 1992 Compact finite difference schemes with spectral-like resolution. *J. Comp. Phys.* **103,** 16-42.

Libby, P. A., Williams, F. A. 1994 Fundamental aspects: a review. In *Turbulent Reacting Flows.* (ed. P. A. Libby & F. A. Williams). Academic Press London, 1-57.

Moin, P., Squires, K., Cabot, W. & Lee, S. 1991 A dynamic subgrid-scale model for compressible turbulence and scalar transport. *Phys. Fluids A.* **3,** 2746-2757.

Müller, C. M., Breitbach, H. & Peters, N. 1994 Partially premixed turbulent flame propagation in jet flames. *Twenty-Fifth Symp. (Intl) on Combust.* The Combustion Institute, 1099-1106.

Muñiz, L. & Mungal, M. G. 1997 Instantaneous flame-stabilization velocities in lifted-Jet diffusion flames. *Combust. Flame.* **111,** 16-31.

Peters, N. 1986 Laminar flamelet concepts in turbulent combustion. *Twenty-first Symp. (Intl) on Combust.* The Combustion Institute, 1231-1250.

Peters, N. & Williams, F. A. 1983 Liftoff characteristics of turbulent jet diffusion flames. *AIAA J.* **21,** 423-429.

Phillips, H. 1965 Flame in a buoyant methane layer. *Tenth Symp. (Intl) on Combust.* The Combustion Institute, 1277.

Pierce, C. D. & Moin, P. 1998 Large eddy simulation of a confined coaxial jet with swirl and heat release. *AIAA Paper 2892* 29th AIAA Fluid Dynamics Conference, Albuquerque NM.

Pitts, W. M. 1988 Assessment of theories for the behavior and blowout of lifted turbulent jet diffusion flames. *Twenty-Second Symp. (Intl) on Combust.* The Combustion Institute, 809-816.

Plessing, T., Terhoeven, P., Peters, N., Mansour, M. S. 1998 An experimental and numerical study of a laminar triple flame. *Combust. Flame.* **115**(3)**,** 335-353.

Poinsot, T. & Lele, S. K. 1992 Boundary conditions for direct simulations of compressible viscous flows. *J. Comp. Phys.* **101,** 104-129.

Poinsot, T., Candel, S. & Trouvé, A. 1996 Direct numerical simulation of premixed turbulent combustion. *Prog. Energy Combust. Sci.* **12,** 531-576.

Pope, S. B. 1985 Pdf method for turbulent reacting flows. *Prog. Energy Combust. Sci.* **11,** 119-195.

Ravet, F. & Vervisch, L. 1998 Modeling non-premixed turbulent combustion in aeronautical engines using PDF-Generator. *AIAA Paper 1027,* 36th Aerospace Sciences Meeting and Exhibit, Reno Nv.

Réveillon, J. & Vervisch, L. 1996 Response of the dynamic LES model to heat release induced effects. *Phys. Fluids.* **8**(8).

Réveillon, J. & Vervisch, L. 1998 Subgrid mixing modeling: a dynamic approach. *AIAA J.* **36**(3)**,** 336-341.

Ruetsch, G. R., Vervisch, L. & Liñán, A. 1995 Effects of heat release on triple flame. *Phys. Fluids.* **7**(6)**,** 1447-1454.

Smith, N. S. 1996 Conditional moment closure of mixing and reaction in turbulent nonpremixed combustion. *Annual Research Briefs.* Center for Turbulence Research, NASA Ames/Stanford Univ., 85-99.

Vanquickenborne, L. & Van Tiggelen, A. 1966 The stabilization mechanism of lifted diffusion flames. *Combust. Flame.* **10,** 59-69.

Vervisch, L. & Poinsot, T. 1998 Direct numerical simulation of non-premixed turbulent flame. *Ann. Rev. Fluid Mech.* **30,** 655-692.

Veynante, D., Vervisch, L., Poinsot, T., Liñán, A., Ruetsch, G. 1994 Triple flame structure and diffusion flame stabilization. *CTR 1994 Summer Proceedings.* Center for Turbulence Research, NASA Ames/Stanford Univ., 55-73.